Biosensors and Bioelectronics 139 (2019) 111321

Contents lists available at ScienceDirect

Biosensors and Bioelectronics

journal homepage: www.elsevier.com/locate/bios

Molecularly imprinted electroluminescence switch sensor with a dual recognition effect for determination of ultra-trace levels of cobalt (II)

Shuhuai Li[a,b,*], Jianping Li[c], Xionghui Ma[a,b], Chaohai Pang[a,b], Guihao Yin[a,b], Jinhui Luo[a,b,**]

[a] Analysis and Test Center of Chinese Academy of Tropical Agricultural Sciences, Haikou, 571101, China
[b] Hainan Provincial Key Laboratory of Quality and Safety for Tropical Fruits and Vegetables, Haikou, 571101, China
[c] College of Chemistry and Bioengineering, Guilin University of Technology, Guilin, 541004, China

ARTICLE INFO

Keywords:
Molecularly-imprinted
Bovine serum albumin-metal
Dual selective
Switch
Electrochemiluminescence

ABSTRACT

A dual selection/recognition effect is described for cobalt (II) ions (Co^{2+}). It is based on bovine serum albumin-metal-Co^{2+} coordination (BSA-Co^{2+}) and the use of a molecularly imprinted polymer (MIP). An electrochemiluminescence (ECL) switch sensor was designed for detecting nanomolar levels of Co^{2+}. The BSA-Co^{2+} coordination complex was chosen as a template to prepare a MIP modified switch sensor. The coordination reaction between BSA and Co^{2+} provides the first step in recognition, and MIP provides the second step for Co^{2+}. This leads to a strong improvement in selectivity of the sensor. A multi-walled carbon nanotube/Cu nanoparticles/carbon quantum dots nanocomposite (MWCNT/Cu/C-dots) acts as an ECL device, and the BSA-Co^{2+} complex quenches the ECL signal. Therefore, the elution and resorption of BSA-Co^{2+} can be used as a switch to control ECL. Additionally, a method was established to detect Co^{2+}, with the detection limit as low as 3.07×10^{-10} mol/L. The method was applied to the analysis of spiked environmental water, soil samples, and agricultural products. The recovery rates of the method were in the range of 87.5–111.3%.

1. Introduction

Cobalt (II) (Co^{2+}) pollution (Jadwiga, 2001) in soil and water is mainly generated from the mining industry, industrial wastewater, and burning of fossil fuels (coal and oil). Co^{2+} pollution in soil or water not only affects growth and yield of agricultural crop plants, but also poses a potential risk to food sources and human health (Afolaranmi et al., 2010). Therefore, it is necessary to effectively monitor even trace amounts of Co^{2+} in the environment and agricultural products. Existing methods for detecting Co^{2+} include atomic absorption spectrometry (Baytak and Türker, 2005), inductively coupled plasma mass spectrometry (Liang et al., 2018), fluorescence methods (Chen et al., 2013; Li et al., 2014), and electrochemical techniques (Maity et al., 2014). However, these methods have certain issues, including serious interference, complicated sample preparation, being time-consuming, involve expensive instruments, and exhibit low sensitivity. Therefore, the establishment of a simple, rapid, sensitive, and specific method for detecting Co^{2+} has become an urgent problem to be resolved.

The molecular imprinting technique (MIT) (Chen et al., 2016) is a new effective separation technique, which can generate a molecularly imprinted polymer (MIP) (And and Mosbach, 2000) featuring selective recognition for specific molecular compounds. Due to its high selectivity, MIP-based sensors have attracted attention in the field of metal ion detection (Bansod et al., 2017; Besharati-Seidani and Shamsipur, 2015; Sun et al., 2018). The means of detection involves using a functional monomer to combine with a metal ion via a coordination bond in order to enable functional monomers in the generated MIP. However, many metal ions are small, and the structural characteristics of different metal ions include closely related structures. Furthermore, ions of the same family as the target analyte ion often have similar chemical properties and may interfere with specific detection (Yang et al., 2017). This causes metal ions to be difficult to imprint in MIP, and it can be challenging to completely removed their influence in MIP sensor-based method. Recent studies show that, metal complexes employed as template molecules to prepare MIP sensors can achieve a dual recognition effect and effectively improve the selectivity of the sensor (Yang et al., 2016). This is because the coordination reaction provides a first layer of recognition, while the molecular imprinting technique can provide a second layer of recognition, thereby effectively increasing the recognition site. Li's group (Li et al. 2015, 2018) reported an MIP sensor which used copper amide and trivalent terbium ion (Tb^{3+})-ethylenediaminetetraacetic acid complex as a

* Corresponding author. Analysis and Test Center of Chinese Academy of Tropical Agricultural Sciences, Haikou, 571101, China.
** Corresponding author. Hainan Provincial Key Laboratory of Quality and Safety for Tropical Fruits and Vegetables, Haikou, 571101, China.
E-mail addresses: happylishuhuai@163.com (S. Li), luocatas@21cn.com (J. Luo).

https://doi.org/10.1016/j.bios.2019.111321
Received 15 February 2019; Received in revised form 6 May 2019; Accepted 12 May 2019
Available online 16 May 2019
0956-5663/

template molecule for Cu^{2+} and Tb^{3+} detection, respectively. The sensor exhibits enhanced selectivity and sensitivity. However, the coordination reaction between metal ions and amide or ethylenediaminetetraacetic acid is much more broadly applicable for metal ions. The coordination complexes have no obvious differences in their structures. This means that the recognition by MIP of metal ion-coordination complexes has significant differences, thus, the ability to rule out interference of MIP sensors is yet to be further improved. Furthermore, such sensors mainly detect electrical current, potential, and microbalance signals. Such signals are generally less stable; and these methods often introduce competing reactions and catalytic amplification of enzyme tags, making the steps involved cumbersome and costly, and are not conducive to practical applications. Bovine serum albuminmetal (BSA) (Chen et al., 2014) can react with metal ions via amino acid residues. After the coordination reaction, the structure of BSA has large variations in conformation and charge distribution, and such complexes have different configurations after different metal ions have coordinated with BSA (Lee et al., 2007; Wu et al., 2008). Hence, it may be a promising strategy to use BSA in the first recognition step for metal ions in MIP sensors. However, there are no reports regarding the use of protein molecular imprinted polymers for metal detection. imprinted.

In this study, BSA-Co^{2+} coordination complex (BSA-Co^{2+}) was introduced as the template molecules in the preparation of MIP. First, a gold electrode surface was modified by a multi-walled carbon nanotube/Cu nanoparticle/carbon quantum dots (MWCNT/Cu/C-dots) nanocomposite. Then, a MIP was prepared on MWCNT/Cu/C-dots modified electrode surface, with BSA-Co^{2+} as a template molecule and *o*-aminophenol as a functional monomer by electrochemical polymerisation. Co^{2+} can react with amino acid residues of BSA, which is referred to as the first recognition step. Specific recognition sites for BSA-Co^{2+} were obtained after eluting BSA-Co^{2+} from the MIP; this is referred to as the second recognition step for Co^{2+}. Hence, the sensor's selectivity for Co^{2+} was improved with a dual recognition effect. At the same time, MWCNT/Cu/C-dots were used as an electroluminescence (ECL) device, and electrically excited and reacted with the co-reactant H_2O_2 to generate an enhanced ECL signal. This ECL signal can be quenched by BSA-Co^{2+}. Thereby, a switching sensor was arrived at, whose ECL intensity is controlled by the elution and adsorption of BSA-Co^{2+} as shown in Fig. 1. When BSA-Co^{2+} was eluted from the MIP, a strong ECL signal was generated, which is referred to as 'switch on'. When BSA-Co^{2+} was re-adsorbed to the MIP, the ECL signal was quenched, which is referred to as 'switch off'. By the above means, a method for detecting trace amounts of BSA-Co^{2+} was established.

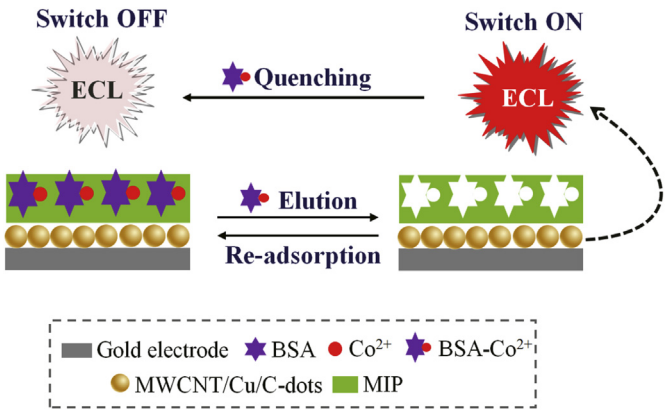

Fig. 1. Procedure for switch sensor fabrication for the detection of Co^{2+}.

2. Materials and methods

2.1. Chemicals, reagents, and apparatus

Cobalt ion standard solution (Co^{2+}, 0.5 mmol/L), Bovine serum albumin analytical standard (BSA, > 98%), and multiwalled carbon nanotube was purchased from Shanghai Aladdin Biotechnology Co., Ltd.; *o*-aminophenol, $CuSO_4$, potassium ferrocyanide, potassium ferricyanide, thioglycolic acid, potassium chloride, and other reagents were purchased from Xilong Scientific Co., Ltd., China. phosphate buffer (PBS) was prepared from Na_2HPO_4 and NaH_2PO_4, containing 0.1 mmol/L NaCl. Unless otherwise specified, the chemicals used in the experiment were of analytical grade and the water was double deionised water (18.2 MΩ, Milli-Q, and Millipore).

CHI-660E electrochemical workstation (Shanghai Chenhua Instrument Co., Ltd., Shanghai, China); MPI-Electrochemiluminescence analysis system (Xi'an Ruimai Analytical Instrument Co., Ltd.); Transmission electron microscopy (TEM) images were acquired with an Axio Imager apparatus (Carl Zeiss AG, Oberkochen, Germany); Scanning electron microscopy (SEM) images were obtained with an Axio Imager scanning electron microscope (Carl Zeiss AG, Oberkochen, Germany); X-ray photoelectron spectroscopy (XPS) was carried out with a VG Multilab 2000spectrometer (Thermo Electron Corporation); Three-electrode system: molecularly imprinted polymer modified gold electrode (d = 2 mm) as the working electrode, the Ag/AgCl electrode as the reference electrode, and the platinum wire electrode as the counter electrode.

2.2. Synthesis of BSA-Co^{2+}

BSA-Co^{2+} was synthesised by a self-assembly method. 2 mL (0.5 mmol/L) Co^{2+} standard solution and 2 mL BSA (0.5 mmol/L) were added to a 4 mL of PBS solution. When fully mixed after 5 min, the solution was purified by dialysis and diluted with PBS to 10 mL, the BSA-Co^{2+} was obtained.

2.3. Synthesis of MWCNT/Cu/C-dots

C-dots were synthesised using a method described in the literature (Guo et al., 2013; Li et al., 2017). First, sodium citrate (0.25 g) and NH_4HCO_3 (2.0 g) and 20 mL ultrapure water were added in a reaction vessel, which was sealed inside a Teflon lined stainless steel autoclave and heated at 200 °C for 3 h, following which the autoclave was allowed to cool to room temperature. Purification of the obtained C-dots was carried out using dialysis tubing. Then, with reference to the literature (Chinnappan et al., 2018; Du et al., 2010) with some modifications, MWCNT (30 mg) and polyvinylpyrrolidone (0.06 g) were dispersed in ultrapure water via ultrasound. Next, 0.10 g C-dots, 5 mL $CuSO_4$ (10 mmol/L) and 200 μL mercaptoacetic acid were added, and stirred for 20 min. The mixture was heated to 180 °C using a high-temperature, high-pressure autoclave for 24 h. After cooling the mixture to room temperature, the solution was centrifuged, and the precipitate was washed several times with distilled water and ethanol. The final product was dried under vacuum at 50 °C for 3 h, yielding the MWCNT/Cu/C-dots nanocomposite.

2.4. Preparation of MIP modified electrodes

The gold electrode was washed with 50% nitric acid, absolute ethanol, and distilled water before use. Then, MWCNT/Cu/C-dots were combined on the gold electrode through thiol base self-assembly. The modified electrode was then placed in a 10 mL sodium acetate buffer solution (pH = 5.3) containing 3 mmol/L *o*-aminophenol and 2 mL BSA-Co^{2+}. Cyclic voltammetry (CV) was performed between 0 V and +0.8 V with a scan rate of 50 mV/s for 20 cycles. After electropolymerisation was completed, the electrode was gently stirred in a

50% methanoic acid mixture for 3 min to remove the template molecule BSA-Co^{2+} molecules and other adsorbates. An MIP sensor with cavities was obtained; this is because MIP adsorbed BSA-Co^{2+}, mainly by amino group and hydrogen bonds. In order to remove the BSA-Co^{2+} effectively, it was necessary to break amino group and hydrogen bonds between the template molecules and MIP. After this, polar solvents such as methanoic acid were able to play a role in breaking hydrogen bonds.The re-adsorption of BSA-Co^{2} was carried out after eluting the template molecules by placing the sensor in BSA-Co^{2} solutions of different concentrations. In addition, the same polymerisation method was used to prepare the non-MIP (NIP) sensor, the only difference being that the template molecule BSA-Co^{2} was not added to the solution for electropolymerisation.

2.5. Electrochemical analysis experimental methods

The conditions of CV detection were set as follows: the scan range was from 0 to 1.0 V, and the scan rate was 50 mV/s. The conditions of electrochemical impedance spectroscopy (EIS) detection were set as follows: the potential was 0.190 V, the frequency range was from 0.1 Hz to 100000 Hz, and the alternating voltage was 5 mV. ECL detection was performed in a 0.1 mol/L PBS (pH 7.8, containing 1 mmol/L H_2O_2) using a three-electrode system. The scan range was from −0.2 to 0.7 V (vs. SCE), the scan rate was 50 mV/s. A 700 V high voltage was supplied for the photomultiplier. The sampling rate was 10 T/s.

2.6. Sample pre-treatment

Different samples were pre-treated in different ways as shown in Supplementary Material.

3. Results and discussion

3.1. Electropolymerisation of MIP

O-aminophenol and BSA-Co^{2+} can combine through the weak hydrogen bonds formed between the amino group and the hydroxyl groups. A distinct irreversible oxidation peak of *o*-aminophenol was observed at 0.58 V, as shown in Fig. S1. As the number of electropolymerisation cycles continued, the oxidation peak continuously reduced. This was because a dense polymer film with poor conductivity formed on the surface of the gold electrode, which hindered the electron transfer. When the number of electropolymerisation cycles reached 20, the peak current had become very small, indicating that the MIP had formed on the electrode surface. If the number of cycles was less than 20, printed capacity became smaller. In contrast, if the number of cycles was more than 20, the eluting effect became worse. Hence, 20 was chosen as the final number of cycles of electropolymerisation.

3.2. MWCNT/Cu/C-dots characterization

The MWCNT/Cu/C-dots composite nanomaterial was analysed using TEM, and XPS. As shown in Fig. 2A, the diameter of the MWCNT was 10–30 nm and the length was 2–4 μm. Cu/C-dots nanoparticles were spherical in shape and had a uniform particle size and good dispersibility, which was observed on the surface of the MWCNT in Fig. 2B. Cu/C-dots have an average particle size of approximately 40 nm, and particle size is mainly distributed in the range of 20–80 nm. Fig. 2C XPS spectrogram shows the elemental composition of MWCNT/Cu/C-dots. The intense peak signals were observed at 285.5 and 286.5 eV, corresponding to C (1s), which is mainly from C-dots and MWCNT. Peaks were observed at 953.3 and 933.5 eV, corresponding to Cu (2p2/3) and Cu (2p1/3) respectively, which are mainly from Cu (Fig. 2D). The above results indicated that the MWCNT/Cu/C-dots nanocomposite had been successfully prepared.

3.3. BSA-Co^{2+} characterization

BSA-Co^{2+} complexes were characterised using ultraviolet spectrum (UV) and XPS. The UV spectrum is shown in Fig. S2, BSA has an obvious absorption peak at 280 nm, and the absorption peak was enhanced after BSA was reacted with Co^{2+} to form BSA-Co^{2+} (curve a to curve b). This is because BSA and Co^{2+} form coordination complexes by means of intermolecular forces, changing the molecular structure of BSA. (Liu et al., 2009). As shown in Fig. S3, BSA exhibited intense peaks corresponding to C (1s) at 288.5 eV, O (1s) at 533 eV, and N (1s) at 397 eV. Peaks corresponding to Co ($2p_{1/2}$) were observed at 795.5 eV and Co ($2p_{3/2}$) at 780.5 eV, which is from Co^{2+}. The above results indicated that BSA-Co^{2+} has been successfully prepared.

3.4. Characterization of MIP

MIP was characterised by CV, EIS, XPS and SEM. As the imprinted cavities on the MIP can serve as channels for electron mass transfer, the plugging or opening of channels can cause a change in the response of the electrode to the redox peak current of the ion probe.

As shown by the CV curve in Fig. 3A, owing to the formation of a MIP on the modified electrode surface, it became difficult for the redox reaction involving $K_3[Fe(CN)_6]/K_4[Fe(CN)_6]$ to occur on the electrode surface. Therefore, the response peak current of the electrode decreased when MWCNT/Cu/C-dots were coated on the electrode surface (curve a to curve b), and the response peak current decreased rapidly when MIP covered the modified electrode (curve b to curve c). After eluting the BSA-Co^{2+}, the channel opening for the proton transfer, and the response peak current again increased (curve c to curve d). When BSA-Co^{2+} was re-adsorbed by MIP, the channels were blocked, resulting in a decrease in the response peak current (curve d to curve e). However, for the NIP, as there was no template molecule in the polymerisation process, the imprinted cavities did not appear after the elution step, so the current hardly changed (curve f to curve g). Fig. 3B shows the surface resistance of the sensor. The inset shows the Randles equivalent circuit model used for EIS analysis. The total electrode impedance corresponded to the electron transfer resistance (Ret) in series with the parallel connection of the double-layer capacitance (Cdl) and Warburg impedance (Zw). In EIS, the semi-circular diameter of EIS equalled the electron transfer resistance, Ret. After the MWCNT/Cu/C-dots were coated onto the electrode surface, the resistance of the sensor was slightly greater than bare gold electrodes (curve a to curve b). When a dense MIP formed on the MWCNT/Cu/C-dots modified gold electrode, the resistance of sensor became large (curve b to curve c). When BSA-Co^{2+} was eluted by the eluent, the electrical resistance was reduced (curve c to curve d), In contrast, when BSA-Co^{2+} was re-adsorbed by MIP, the imprinted cavities were blocks, and the resistance of the sensor became larger again (curve d to curve e). As shown in Fig. 3C of the XPS spectrum, the Co ($2p_{1/2}$) peak at 795.5 eV and Co ($2p_{3/2}$) peak at 780.5 eV, mainly from BSA-Co^{2+}, disappeared after BSA-Co^{2+} was removed from the MIP (curve a to curve b); At the same time, the peak of C (1s), O (1s), and N (1s) at 288.5 eV, 533 eV, and 397 eV declined. The above results indicated that the MIP sensor had been successfully prepared. SEM graphics are shown in Fig. S4. The surface of the gold electrode was smooth (Fig. S4A), and MWCNT/Cu/C-dots were spread over the electrode surface. MWCNT has long ribbon-like shape, and Cu/C-dots were predominantly spheroidal particles (Fig. S4B). The MIP on the surface of the modified electrode were compact, with no obvious cavity (Fig. S4C). After eluting the BSA-Co^{2+}, cavity shadows appeared on the MIP (Fig. S4D).

3.5. ECL response and mechanism of the sensor

The ECL response of the sensor was investigated. As shown in Fig. 4, C-dots on the gold electrode surface were able to produce an obvious ECL signal (curve a), and the ECL signal of MWCNT/Cu/C-dots was

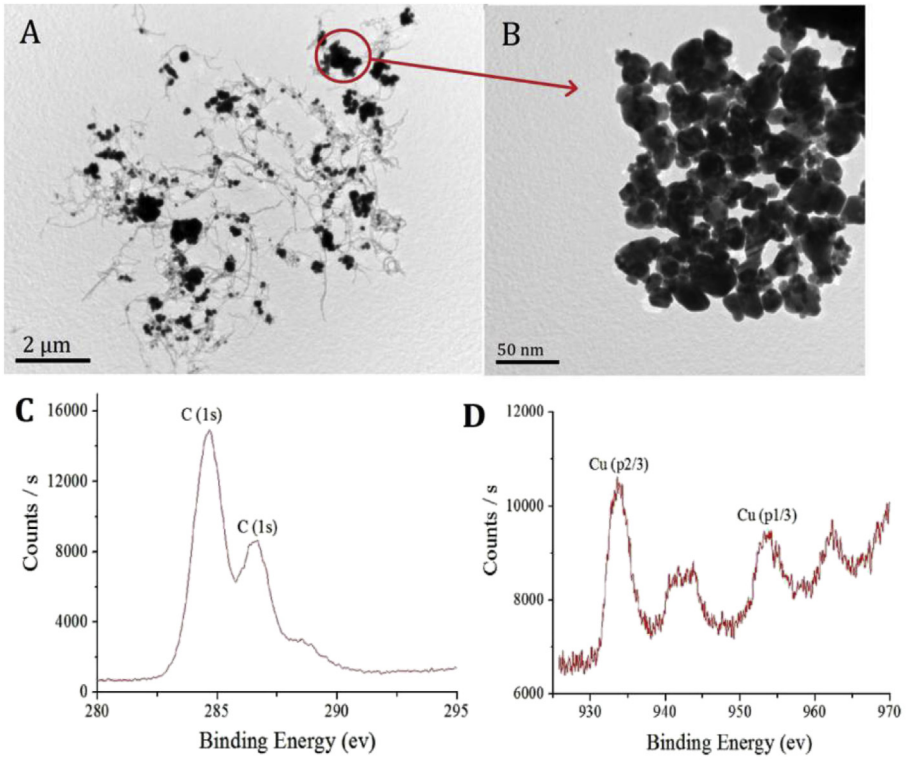

Fig. 2. (A) TEM of MWCNT/Cu/C-dots; (B) TEM of Cu/C-dots; (C)XPS of MWCNT/Cu/C-dots; (D) XPS of Cu/C-dots.

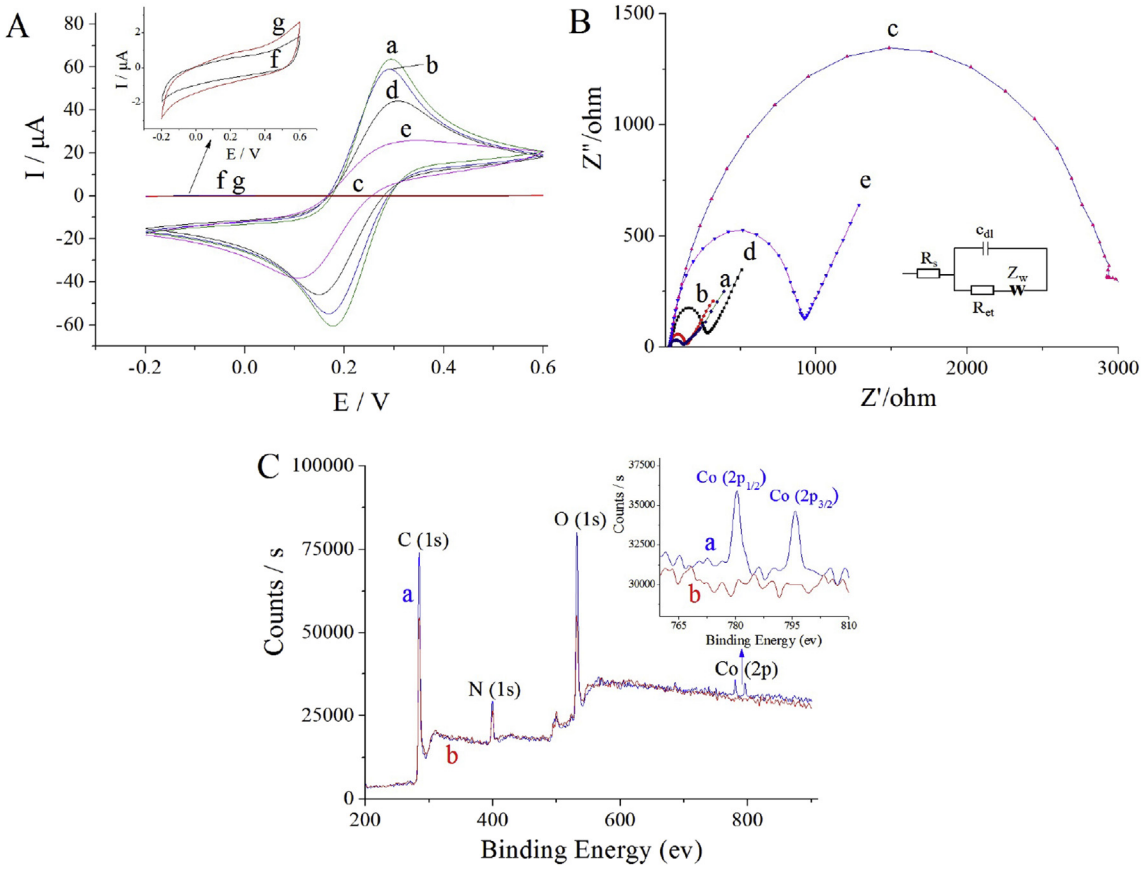

Fig. 3. CV (A) and EIS (B) of the sensor under different conditions: a. bare gold electrode; b. MWCNT/Cu/C-dots modified gold electrode; c. MIP modified electrode; d. MIP modified electrode after the removal of BSA-Co^{2+}; e. MIP modified electrode after the rebinding of BSA-Co^{2+}; f. NIP modified electrode; g. NIP modified electrode after the removal of BSA-Co^{2+}; (C) XPS of MIP: a. MIP modified electrode; b. MIP modified electrode after the removal of BSA-Co^{2+}. (For interpretation of the references to colour in this figure legend, the reader is referred to the Web version of this article.)

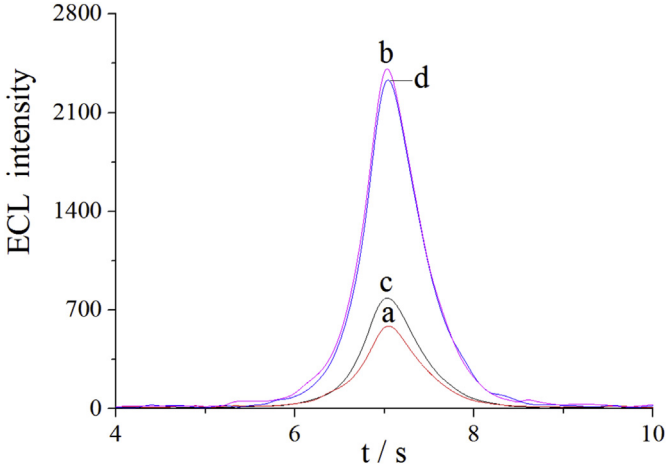

Fig. 4. ECL response of sensor under different conditions: a. ECL intensity of C-dots; b. ECL intensity of MWCNT/Cu/C-dots; c. ECL intensity of MIP modified electrode; d. ECL intensity of MIP modified electrode after BSA-Co^{2+} removed.

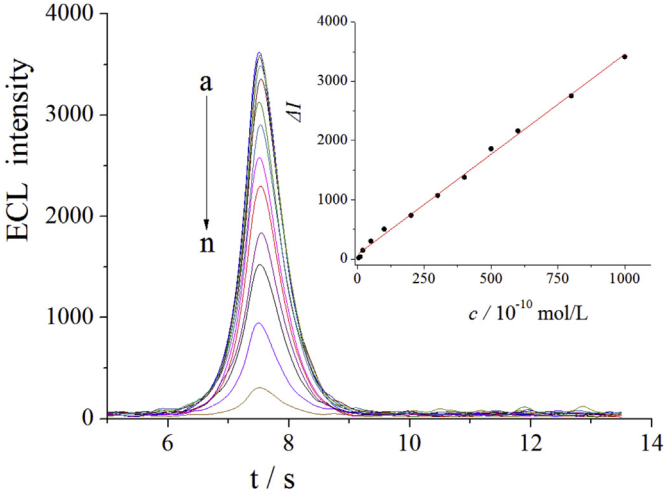

Fig. 5. ECL response of the sensor re-adsorbed BSA-Co^{2+} at different concentrations. a–l: (0, 10, 20, 50, 100, 200, 300, 400, 500, 600, 800, 1000) × 10^{-10} mol/L Co^{2+}.

enhanced significantly compared to that of C-dots (curve b). This is because MWCNT/Cu has a relatively larger specific surface areas and photoelectric properties. When the MIP was polymerised onto the surface of the MWCNT/Cu/C-dots modified gold electrode with 8×10^{-10} mol/L Co^{2+}, the ECL signal of the sensor was significantly reduced (curve c). This is because BSA-Co^{2+} effectively quenched the luminescence intensity of the C-dots. The mechanism of ECL may be that the C-dots lose electrons after being excited, the electrons are transferred to the co-reagent H_2O_2, and further reactions occur to form an excited state (Xu et al., 2014). After returning from the excited state to the ground state, optical radiation is generated. When BSA-Co^{2+} was adsorbed onto MIP, Co^{2+} was able to catalyse the decomposition reaction of H_2O_2 (Hanif et al., 2016); and the ECL resonance energy transfer between C-dots and Co^{2+} could further quench the ECL intensity. In this system, the electrons excited during H_2O_2 concentration catalysis were accepted by Co^{2+}, thus no further reactions occurred, which affected the generation of ECL signals. However, when BSA-Co^{2+} was removed form MIP, this blocking effect disappeared, and the ECL intensity recovered (curve d).

3.6. Optimisation of detection conditions

The following parameters were optimised as described in Supplementary Material: (a) pH of the PBS buffer; (b) elution time; and (c) re-adsorption time. ECL intensity was measured under different conditions. The corresponding data are shown in Fig. S5 and Fig. S6. The following experimental conditions were found to give the best results: (a) a PBS buffer pH value of 7.8; (b) 8 min as the elution time; and (c) 5 min as the re-adsorption time.

3.7. Calibration curve

The calibration curve of Co^{2+} concentration and ECL signal intensity change is shown in Fig. 5. First, Co^{2+} was reacted with BSA to form BSA-Co^{2+} coordination complexes, then adsorbed to the recognition sites on the sensor, and the ECL signal was detected. Over Co^{2+} concentration range of 10–1000 × 10^{-10} mol/L, the ECL intensity difference ΔI exhibited a good linear relationship with the concentration of Co^{2+} standard solution c. The linear equation can be expressed as $\Delta I = 2.23\ c\ (10^{-11}$ mol/L) + 5.97,with a correlation coefficient of $r = 0.998$. The detection limit of the method reached 3.07×10^{-10} mol/L ($LOD = 3\delta b/K$). Compared with other methods, this method showed great advantages in terms of detection limit and detection range, as shown in Table S1.

3.8. Sensor selectivity, reproducibility and stability

The selectivity of the sensor for Co^{2+} was investigated under optimised experimental conditions. Changes in the ECL intensity response were compared in the 1.0×10^{-8} mol/L Co^{2+} solution and the mixed solution of Co^{2+} (1.0×10^{-8} mol/L) included 1.0×10^{-5} mol/L Ca^{2+}, Ag^{+}, Sn^{2+}, Mg^{2+}, Ni^{2+}, Hg^{2+}, Zn^{2+}, Pb^{2+}, Cd^{2+}, Fe^{3+}, Cr^{3+}, Mn^{2+}, and Fe^{2+}. The results showed that the relative deviations of two measurements were within 5% (Fig. S6). This showed that general metal ions exerted no interference in the experiment. Some metal ions have similar structures to like Co^{2+}, when they are coordinated with the same complexing agent. However, these complexes had different bond lengths and bond angles, i.e., different spatial configurations. This resulted in differences when the complexes were recognised by the MIP. The specific recognition sites on the MIP were able to specifically recognise BSA-Co^{2+} but had poor recognition ability for other complexes of different spatial configurations, thereby eliminating interference. Compared with the imprinted membrane that recognises a single metal ion species, the sensor developed in this study had distinct structural characteristics due to the metal ion complexation reaction that allowed it to recognise ions via the imprinted membrane, thereby improving its sensitivity.

The reproducibility test of the sensor was carried out by examining the sensor's ECL signal after reacting it with 1.0×10^{-8} mol/L Co^{2+}. First, the ECL signal was measured five times for the same sensor. The relative standard deviation was 2.65%. Then the ECL response signals of five identical sensors were examined. The relative standard deviation of the ECL response values of the five sensors was found to be 3.95%. The above results indicated that the sensor had good reproducibility. The sensor was stored in a 4 °C refrigerator when not in use. To examine the stability of the molecularly imprinted sensor, changes in the ECL response values were detected periodically. There was almost no change in ECL signal intensity over 10 days, and the ECL signal intensity decreased by 7.68% after 20 days. The above results showed that the sensor exhibited good stability.

3.9. Detection of Co^{2+} in samples

The pre-treated samples are described in Supplementary Material. Then MIP sensor was used to re-adsorb target molecules after the elution process. The results are shown in Table 1. The recovery rate of the MIP sensor was between 87.5% and 111.3%, and the relative standard deviation (RSD) was less than 5.0%, which demonstrates that the MIP

Table 1
Results of sample assay and recoveries.

Samples	This method 10^{-9} mol/L (n = 5)	RSD %	HPLC-ICP-MS method 10^{-9} mol/L (n = 5)	Added 10^{-9} mol/L	Total found 10^{-9} mol/L (n = 5)	RSD %	Recoveries %
Surface water	Not detected	–	Not detected	5.00	5.45	3.88	109.0
Industrial sewage	9.65	4.56	9.76	5.00	14.25	4.98	92.0
Agricultural soil	Not detected	–	Not detected	10.00	9.04	4.52	90.4
Chinese cabbage	Not detected	–	Not detected	10.00	8.75	3.66	87.5
broccoli	Not detected	–	Not detected	15.00	16.7	4.12	111.3

sensor had good recovery rates and practicability.

4. Conclusions

In this study, the recognition of the metal complex BSA-Co^{2+} and the recognition of MIP were combined in a sensor, thereby improving the sensor's ability to selectively recognise Co^{2+}. Due to the dual recognition effect, the sensor can effectively eliminate interference from other metal ions. MIP can be repared with different coordinate complexes (BSA reacted with different metal ions) as template molecules; in this way, this method can be applied to the detection of different heavy metal contaminants. The proposed label-free ECL switch detection method exhibited the following features: a simple detection process, stable detection signals, high detection limits, and high sensitivity. It also showed strong applicability in the detection of ultra-trace Co^{2+} levels in environmental water, soil samples, and agricultural products.

Declaration of interests

The authors declare that they have no known competing financial interests or personal relationships that could have appeared to influence the work reported in this paper.

CRediT authorship contribution statement

Shuhuai Li: Writing - original draft. **Jianping Li:** Formal analysis. **Xionghui Ma:** Formal analysis. **Chaohai Pang:** Formal analysis. **Guihao Yin:** Formal analysis. **Jinhui Luo:** Writing - original draft.

Acknowledgements

This project was supported by the Central Public-interest Scientific Institution Basal Research Fund for the Chinese Academy of Tropical Agricultural Sciences (No.1630082017002 and 1630082019003).

Appendix A. Supplementary data

Supplementary data to this article can be found online at https://doi.org/10.1016/j.bios.2019.111321.

References

Afolaranmi, G.A., Henderson, C., Grant, M.H., 2011. Toxicol. In Vitro 25, 125–130.
And, K.H., Mosbach, K., 2000. Chem. Rev. 100, 2495–2504.
Bansod, B.K., Kumar, T., Thakur, R., Rana, S., Singh, I., 2017. Biosens. Bioelectron. 94, 443–455.
Baytak, S., Türker, A.R., 2005. Microchim. Acta 149, 109–116.
Besharati-Seidani, A., Shamsipur, M., 2015. Microchim. Acta 182, 1747–1755.
Chen, H., Kong, J., Yuan, D., Fu, G., 2014. Biosens. Bioelectron. 53, 5–11.
Chen, H., Yuan, F., Xu, J., Zhang, Y., Wu, Y., Wang, L., 2013. Spectrochim. Acta A Mol. Biomol. Spectrosc. 107, 151–155.
Chen, L., Wang, X., Lu, W., Wu, X., Li, J., 2016. Chem. Soc. Rev. 45, 2137–2211.
Chinnappan, A., Lee, J.K.Y., Jayathilaka, W.A.D.M., Ramakrishna, S., 2018. Int. J. Hydrogen Energy 43, 721–729.
Du, D., Chen, W., Zhang, W., Liu, D., Li, H., Lin, Y., 2010. Biosens. Bioelectron. 25, 1370–1375.
Guo, Y., Wang, Z., Shao, H., Jiang, X., 2013. Carbon 52, 583–589.
Hanif, S., John, P., Gao, W., Saqib, M., Qi, L., Xu, G., 2016. Biosens. Bioelectron. 75, 347–351.
Jadwiga, O., 2001. Microchim. Acta 137, 157–162.
Lee, V.E., Schulman, J.M., Stiefel, E.I., Lee, C.C., 2007. J. Inorg. Biochem. 101, 1707–1718.
Li, C.L., Huang, C.C., Periasamy, A.P., Roy, P., Wu, W.C., Hsu, C.L., Chang, H.T., 2014. RSC Adv. 5, 2285–2291.
Li, J., Yang, B., Pan, H., Xu, G., 2018. Biosens. Bioelectron. 109, 224–229.
Li, J., Zhang, L., Wei, G., Zhang, Y., Zeng, Y., 2015. Biosens. Bioelectron. 69, 316–320.
Li, S., Li, J., Luo, J., Zhang, Q., Zhang, L., 2017. RSC Adv. 7, 56359–56364.
Liang, F., Shi, S., Chen, X., Xie, H., 2018. Microchem. J. 139, 236–241.
Liu, H., Xu, Z., Liu, H., Xi, P., Zeng, Z., 2009. Chem. Pharm. Bull. 57, 1237–1242.
Maity, D., Gupta, R., Gunupuru, R., Srivastava, D.N., Paul, P., 2014. Sensor. Actuator. B Chem. 191, 757–764.
Sun, Y., Jia, M., Yang, J., Huang, Y., Liu, Z., Aisa, H., 2018. Anal. Bioanal. Chem. 410, 349–359.
Wu, L.Z., Ma, B.L., Zou, D.W., Tie, Z.X., Wang, J., Wang, W., 2008. J. Mol. Struct. 877, 44–49.
Xu, Y., Liu, J., Gao, C., Wang, E., 2014. Electrochem. Commun. 48, 151–154.
Yang, B., Li, J., Zhang, L., Xu, G., 2016. Analyst 141, 5822–5828.
Yang, J., Zhang, Y., Zhang, L., Wang, H., Nie, J., Qin, Z., Li, J., Xiao, W., 2017. Chem. Commun. 53, 7477–7480.